Intelligent Efficient Control for Brushless Doubly-Fed Induction Machines

Hamidreza Mosaddegh-Hesar, *Member, IEEE*, Xiaodong Liang, *Senior Member, IEEE*, Hossein Abootorabi Zarchi, Mojtaba Ayaz Khoshhava, *Member, IEEE*, and Amir Khazaee

***Abstract*—In this article, a novel high-efficient control based on brain emotional learning for a brushless doubly-fed induction machine (BDFIM) drive is proposed without requiring a detailed machine model. The step change of the control winding (CW) flux for a given torque and speed is the basis of the proposed controller. The control algorithm detects a steady-state condition by monitoring the speed continuously and then adjusts the CW reference flux's magnitude to determine the minimum total stator current. The stator current is the sum of the current magnitudes at power and control windings of a BDFIM. This model-free intelligent controller has a simple structure and is independent of the machine parameters and robust to disturbances. The proposed control scheme is assessed by a TMS320F2833 microcontroller synchronized with a personal computer for a 3-kW prototype D132s-BDFIM.**

***Index Terms*—Brushless doubly-fed induction machine (BDFIM), flux, intelligent controller, the maximum torque per ampere (MTPA).**

Nomenclature

$\vec{V}$, $\vec{I}$, $\vec{\psi}$	Voltage (V), current (A), flux linkage (Wb) vectors
PW, CW	Power winding, control winding
T	Torque (N·m)
R	Resistance (Ω)
L	Inductance (H)
L_m	Mutual inductance (H)
p	Pole pair number
ω	Angular speed (rad/sec)
ω_n	Natural speed (rad/sec)
s	Slip
T_{samp}	Sampling time (sec)
k, n	Discrete values
A, O	Output node in the network structure of the amygdala and orbitofrontal cortex
E	Output node
V, W	Weights of node
S	Sensory input
S_{th}	Thalamic stimulus
$\gamma, \delta, \gamma_{\text{th}}$	Learning steps in amygdala and orbitofrontal cortex
R_e	Emotional cue function at each time
e	System error
E_p	System output
$E_{\max}$	Maximum output
k_1, K_1, k_2, K_2	Controller gains

Subscripts

1, 2, r	Power winding, control winding and rotor
α, β	Stationary frame axis
d, q	Rotating d-q frame axis

Manuscript received 24 August 2023; revised 27 November 2023, 14 February 2024, and 28 March 2024; accepted 28 April 2024. This work was supported by the Natural Science and Engineering Research Council of Canada (NSERC) Discovery under Grant RGPIN-2016-04170. *(Corresponding author: Xiaodong Liang.)*

Hamidreza Mosaddegh-Hesar and Xiaodong Liang are with the Department of Electrical and Computer Engineering, University of Saskatchewan, Saskatoon, SK S7N 5A9, Canada (e-mail: pvt356@mail.usask.ca; xil659@mail.usask.ca).

Hossein Abootorabi Zarchi is with the Department of Electrical Engineering, Faculty of Engineering, Ferdowsi University of Mashhad, Mashhad 9177948974, Iran (e-mail: abootorabi@um.ac.ir).

Mojtaba Ayaz Khoshhava is with the Department of Electrical Engineering, École de Technologie Supérieure (ÉTS), Montreal, QC H3C 1K3, Canada (e-mail: mojtaba.ayaz@ieee.org).

Amir Khazaee is with the Department of Electrical and Computer Engineering, Toronto Metropolitan University, Toronto, ON M5B 2K3, Canada (e-mail: amir.khazaee@torontomu.ca).

Color versions of one or more figures in this article are available at https://doi.org/10.1109/TIE.2024.3398669.

Digital Object Identifier 10.1109/TIE.2024.3398669

I. Introduction

BRUSHLESS]doubly-fed induction machines (BDFIMs) have a lower capital cost and less harmonic distortions at the machine terminal due to their partially rated frequency converter than singly-fed machines. Compared with doubly-fed induction machines (DFIMs), the elimination of brushes, slip rings, and rotor windings in a BDFIM reduces maintenance costs and the probability of fault occurrence [1]. An explanatory picture of each machine's structure is shown in Fig. 1.

A BDFIM can be operated as an adjustable synchronous machine, where the converter on the control winding (CW) serves as an exciter or can be operated as an asynchronous machine during the converter failure (its performance is relatively poor). Due to a complex structure, a BDFIM's control is complicated. Although several well-known control approaches (the field-oriented control (FOC) [2], [3], [4] and the direct torque control (DTC) [5]) have been investigated for BDFIMs, more advanced control methods, such as the maximum torque per ampere (MTPA) control, are urgently needed.

The MTPA control can be classified into two strategies: 1) the *model-based* method, where the machine model is used to minimize the stator current's magnitude for a given torque (it is simple to implement, but requires the machine parameters); and 2) the *search-based* method, where a control variable that affects the stator current's magnitude is varied step by step to

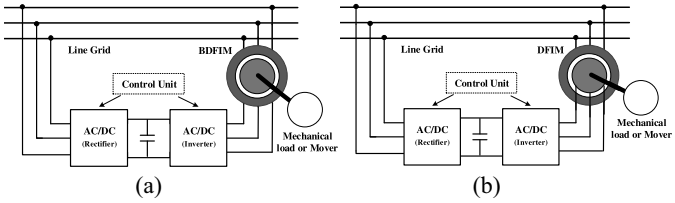

Fig. 1. Simplified view of (a) a BDFIM, (b) a DFIM.

minimize the stator current for a given torque and a given rotor speed (it is independent of the machine parameters, and suitable for applications that do not require fast responses as the flux regulation limits the dynamic performance of the drive).

Extensive research on energy savings has been conducted through model- or search-based MTPA control techniques for singly-fed electric machines [6], [7], [8], [9] but not for BDFIMs. Among few papers for doubly-fed electric machines, Betz et al. in [10] introduced two model-based control strategies, the maximum torque per inverter ampere (MTPIA) and the maximum torque per total ampere (MTPTA), for brushless doubly-fed reluctance machine (BDFRM); conditions to use them in variable speed drives are derived. However, only MTPIA in the BDFRM drive was studied in the subsequent research [11], [12], [13]. By realizing the MTPIA control under a constant torque constraint, the minimum inverter loading can be achieved, but MTPIA can only be applied to CW, so it is not possible to minimize the total stator current. The MTPTA strategy enables the current sharing between windings appropriately for a given torque. In [14], the MTPTA strategy based on the BDFIM model is introduced and the condition to realize it is determined. Although iron losses are generally neglected for MTPA control, the MTPTA strategy considering iron losses is developed by a BDFIM loss model in [15].

The MTPA control is usually implemented by proportional-integral (PI) controllers. PI controllers require tuning and have parameter dependency, but some nonlinear methods, such as the sliding mode control (SMC) [16] and the input–output feedback linearization (IOFL) [14], can overcome these issues. SMC can reject certain uncertainties by knowing the grouped uncertainties and system boundaries, but SMC's stabilization time is not finite and the chattering appears on the system-controlled states [17]. IOFL can transform a nonlinear system to an equivalent linear system, so a linear controller can be developed for it with its inputs determined by a decoupling matrix, but an IOFL controller has internal dynamic issues and may lose stability under steady-state and transient operations.

Over the last two decades, artificial intelligence (AI) methods including rule-based fuzzy logic (FL), neural networks (NN), and genetic algorithm (GA) (evolutionary computing based on genetic principles) have been used for electric machine drives [18], and FL and NN have taken the largest share among all AI methods. A computationally intelligent control system, known as "intelligent controller," is defined as a control system with the learning capability [19].

The brain emotional learning-based intelligent controller (BELBIC) was first proposed by Lucas in 2004 [20] and has been used in various control systems. The BELBIC technique is essentially an action-generation mechanism based on sensory inputs and emotional cues. In an electric drive, sensory inputs (feedback signals) are selected for the control judgment, while emotional cues are selected depending on the performance objectives in practical applications. In [21], the BELBIC is developed on the field-programmable gate array (FPGA) for the mobile crane control. For the first time, the BELBIC for the electric machine control was implemented in [22], where a BELBIC-based speed controller for an interior permanent magnet synchronous motor (IPMSM) was compared with a proportional-integral-derivative (PID) controller, and BELBIC showed excellent features including simple implementation, robustness to disturbances and parameter variations, and very fast response. To modify transient states and improve dynamic responses in the indirect torque control of switched reluctance motors (SRMs), the BELBIC is proposed in cascade with a PI controller in [23]. In [24], the BELBIC is used for accurate speed tracking in a hybrid stepper motor, showing the fast response, negligible overshoots, the minimal deviation from the reference, and zero steady-state errors. In [25], the BELBIC is used through emotional signs and sensory inputs for a synchronous reluctance motor. In [26], a new structure, known as the brain affective system inspired controller, is proposed by considering sensory cortex and modifying computational equations. A permanent magnet synchronous motor (PMSM) drive using brain affective system inspired controller is compared with that using BELBIC and PI controllers through simulation and experiments. In [27], a direct torque and flux control system is proposed for dual stator winding induction machine (DSWIM) based on brain emotional learning. In the proposed DSWIM-drive system the reference values for d- and q- axis voltages of stator winding sets are determined through the proposed controller to directly control flux and torque of each winding sets.

In this article, a novel model-free control method by combining a search-based online MTPA algorithm and an emotional intelligent controller (EIC) is proposed for the BDFIM drive and is validated by simulation and experiments. It is suitable for variable speed applications of BDFIMs, such as pumps. The main contributions of this article include:

1) A BDFIM is complicated due to its unique rotor structure and a large number of degree of freedom, so it is very difficult to design a MTPA controller for BDFIMs. All existing MTPA controllers for BDFIMs in the literature use simplified reduced-order machine models, which decreases the MTPA control's accuracy. In this article, for the first time, a model-free MTPA controller for BDFIMs is developed, where the total stator current is chosen as the objective function, and the CW flux's magnitude is determined by minimizing this objective function using a search algorithm. The proposed control strategy is simple to implement, and is independent of the machine model.
2) An intelligent control technique is proposed based on the brain emotional learning, realized in the power winding (PW) flux's reference frame as two independent controllers, one for the CW flux and the other for the electromagnetic torque implemented on the direct (d)- and

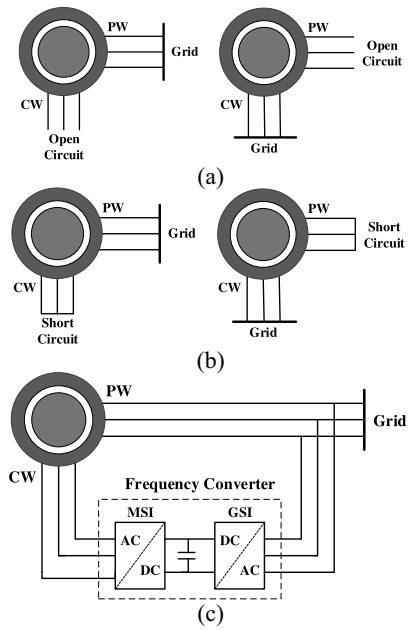

Fig. 2. BDFIM structure. (a) Induction mode. (b) Cascade mode. (c) Synchronous mode.

quadrature (q)-axis, respectively. The proposed brain emotional learning (BEL)-based controller is relatively simple with a reward function to imitate emotional behaviors. It offers ripple free operations and a model-independent structure. Multiple adjustable parameters also enable flexible tuning of the controller based on the desired operations.

3) To implement the MTPA control, it is required to generate the torque reference for the inner control loop. In this article, the BEL-based controller is designed for the speed control loop without needing conventional controllers (PI or PID controllers) for the rotor speed control.

The article is organized as follows: Section II introduces the principle and model of BDFIMs. The algorithm of the MTPA control is proposed in Section III. Section IV presents the principle of the emotion-processing mechanism-based intelligent controller. In Section V, experimental and simulation results are presented. The conclusion is drawn in Section VI.

II. The Basic Principle and Model of BDFIMs

A. The Basic Principle

A BDFIM is a single-frame brushless induction machine with two balanced three-phase windings (PW and CW) placed on its stator. To prevent direct magnetic coupling between them, their pole pairs must be different [28]; to reduce the unbalanced magnetic pull, which is a major source of vibrations and acoustic noises, the difference between their pole pairs must be larger than one [29]. The rotor of a BDFIM has a special cage structure with a number of poles or nests, and its number of pole pairs is equal to the sum of pole pairs of PW and CW. There are three operational modes of a BDFIM, and connections of BDFIM's stator windings are shown in Fig. 2.

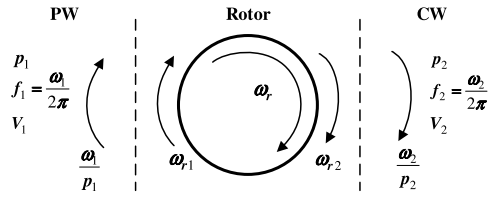

Fig. 3. BDFIM concept: rotational directions of the main magnetic field components [32].

By connecting PW or CW to the power supply, while leaving another stator winding open-circuited [Fig. 2(a)], a BDFIM works as a standard induction machine with p_1 or p_2 pole pairs, respectively. However, operating in this mode leads to a poor performance because the second stator magnetizing inductance is in series with the rotor leakage inductance. If the unexcited PW or CW stator winding is short-circuited or connected to a resistor, while another stator winding is connected to a balanced three-phase supply [Fig. 2(b)], a BDFIM behaves similar to a self-cascaded induction machine. This mode is usually used in starting and accelerating toward the synchronous speed. In the first two operating modes, the rotor speed depends on the rotor's mechanical loading and the power supply frequency.

The third mode of operation, also the most desirable one, is the synchronous mode, in which PW is connected to the power grid directly, and CW is supplied through a partially rated frequency converter [Fig. 2(c)]. The converter consists of two back-to-back voltage source inverters. The inverter connected to the CW, or the machine-side inverter (MSI), controls the CW current; due to the cross-coupling between CW and PW, it also affects the PW current. The grid side inverter (GSI) controls the dc-link voltage [30].

The machine operates at the synchronous mode when the voltage induced in the rotor nested-loops by the PW magnetic field matches the voltage induced in the rotor nested loops by the CW magnetic field. Both magnetic field components associated with the same frequency with an equal phase delay between rotor nests [31]. The rotor produces two main harmonic rotating field components, coupling with PW and CW (Fig. 3).

B. The Model of BDFIMs

The voltage equations of a BDFIM in the $p1$ pole pair synchronously rotating reference frame include

$$\vec{V}_1 = R_1\vec{I}_1 + d\vec{\psi}_1/dt + j\omega_1\vec{\psi}_1 \tag{1}$$

$$\vec{V}_2 = R_2\vec{I}_2 + d\vec{\psi}_2/dt + j(\omega_1 - (p_1+p_2)\omega_r)\vec{\psi}_2 \tag{2}$$

$$\vec{V}_r = 0 = R_r\vec{I}_r + d\vec{\psi}_r/dt + j(\omega_1 - p_1\omega_r)\vec{\psi}_r. \tag{3}$$

The flux space vectors can also be defined as follows:

$$\vec{\psi}_1 = (L_1 + L_{m1})\vec{I}_1 + L_{1r}\vec{I}_r \tag{4}$$

$$\vec{\psi}_2 = (L_2 + L_{m2})\vec{I}_2 + L_{2r}\vec{I}_r \tag{5}$$

$$\vec{\psi}_r = (L_r + L_{m1} + L_{m2})\vec{I}_r + L_{1r}\vec{I}_1 + L_{2r}\vec{I}_2. \tag{6}$$

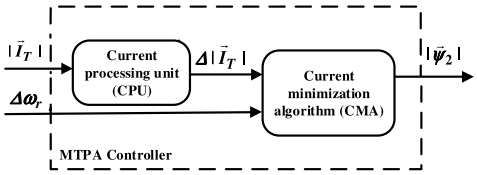

Fig. 4. Simplified block diagram of the proposed MTPA controller.

The model of a BDFIM is similar to the well-known vector model of a standard induction machine. The transformation frequencies of coordinates from CW and the rotor to the PW flux frame are $(p_1+p_2)\omega_r-\omega_1$ and $p_1\omega_r-\omega_1$, respectively.

The electromagnetic torque can be expressed by

$$T_e = 3p_1/2Im\{\vec{\psi}_1^{*}\vec{I}_1\} + 3p_2/2Im\{\vec{\psi}_2\vec{I}_2^{*}\}. \quad (7)$$

Under synchronous conditions and by referring to Fig. 3 [30]

$$\omega_1 - p_1\omega_r = -(\omega_2 - p_2\omega_r). \quad (8)$$

So, the rotor speed is related to the electrical angular speeds of PW and CW as follows:

$$\omega_r = \frac{\omega_1+\omega_2}{p_1+p_2}. \quad (9)$$

This leads to a definition of slips for PW and CW below [32]

$$s_1 \triangleq (\omega_1 - p_1\omega_r)/\omega_1 = \omega_{r1}/\omega_1 \quad (10)$$

$$s_2 \triangleq (\omega_2 - p_2\omega_r)/\omega_2 = \omega_{r2}/\omega_2. \quad (11)$$

III. Intelligent Efficient Control for BDFIMs

A. The Proposed MTPA Controller

In principle, a MTPA control strategy aims to deliver the electromagnetic torque with the lowest current magnitude. To implement the MTPA concept in BDFIMs, the torque equation can be used by setting the optimal current angle value (Appendix I). However, in the proposed search-based MTPA strategy, without needing to know the torque equation, the minimum value of the total stator current for a given load torque is obtained by adjusting the CW's flux. A block diagram of the proposed MTPA controller is shown in Fig. 4, including a current processing unit (CPU) and a current minimization algorithm (CMA). The CPU receives one of the two input signals to the MTPA controller, the total stator current, $|\vec{I}_T|$. $|\vec{I}_T|$ is subject to the averaging and smoothing processes before being applied to the CPU. The CPU then determines the change in $|\vec{I}_T|$, $\Delta|\vec{I}_T|$, over a certain time interval. *Note*: $\Delta|\vec{I}_T|$ is calculated at each sampling step, and thus, represents the difference between the current and previous values of the total stator current at each instance (e.g. $|\vec{I}_T|^0$ and $|\vec{I}_T|^1$ for the first sampling step). The CMA aims to determine the steady-state speed of the rotor, and minimize the total stator current. As the core of the MTPA controller, the CMA is responsible for making proper decisions based on the two signals it receives, $\Delta|\vec{I}_T|$ and the speed error ($\Delta\omega_r$). Under steady-state conditions, the CMA produces the optimal value of CW flux corresponding to a minimum total stator current as its output signal.

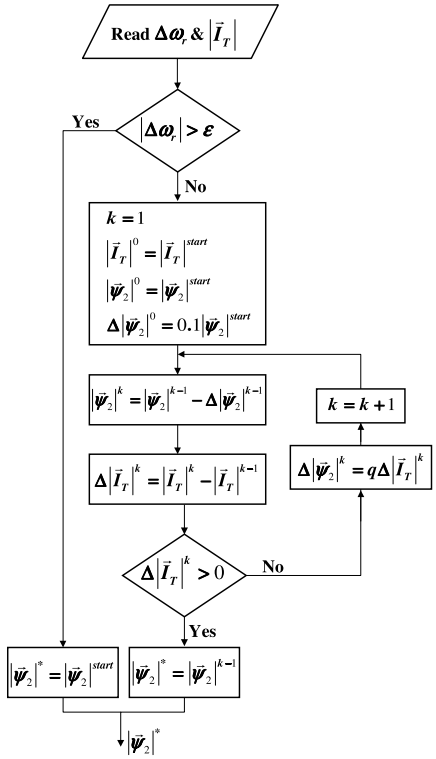

Fig. 5. Proposed search-based MTPA algorithm.

The speed error, $\Delta\omega_r$, in the time interval is continuously monitored by the CMA unit. When it is less than a certain value (ε) for three consecutive measurements, it indicates that the rotor speed has reached a steady state, the CMA then registers and reveals this steady-state rotor speed. After that, the CMA starts to reduce the CW's flux reference from its nominal value step by step, so that the total stator current finally reaches the minimum. By choosing the CW's flux step as large as possible, the system's dynamic response can be improved, but a very large step may cause the system instability, so caution should be exercised when choosing the maximum step size [33]. If the speed error is higher than ε, a transient condition, such as a load torque change, is recognized, and the CW reference flux is set to its start value. Once the machine reaches a new steady state, the CMA is activated again and the total stator current is minimized for the new condition. The flowchart of the proposed searched-based MTPA algorithm is depicted in Fig. 5.

B. The BEL-Based Intelligent Controller

In this article, a computational model based on the limbic system of the mammalian brain and its learning process is proposed for BDFIMs. The MTPA controller generates the optimal flux needed to realize the MTPA strategy; while the BEL-based controller zeros out the errors of torque, speed and flux with respect to their reference values.

The limbic system is one of the most substantial and complicated parts of the human body and comprised of various units, including amygdala, orbitofrontal cortex, thalamus, and sensory cortex. The relationship between the stimulus and emotional consequences is established in amygdala. As a section of the

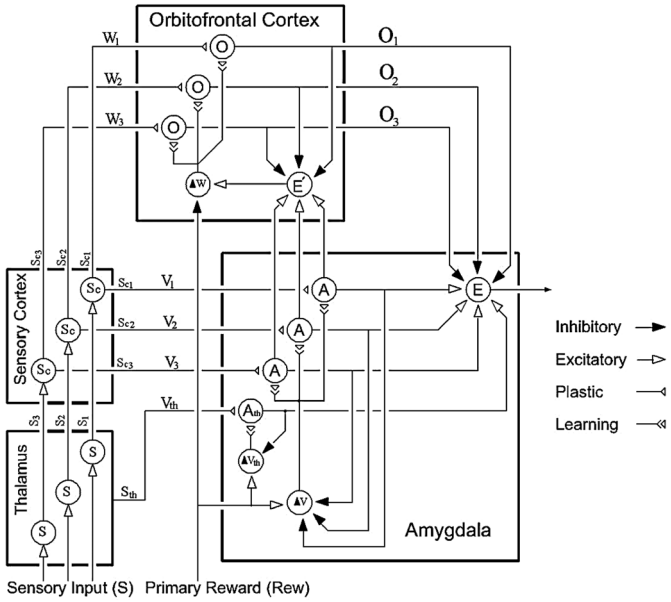

Fig. 6. Network model of the BEL-based controller [18].

brain, amygdala is responsible for the emotional processing and communicating with sensory cortex, thalamus and orbitofrontal cortex. In the computational model, amygdala and orbitofrontal cortex have a network structure, as shown in Fig. 6, where sensory inputs are fed into thalamus, and the maximum of all inputs enters amygdala as a signal. In amygdala, for each sensory input, there is an A node; and in orbitofrontal cortex, there is an O node for each stimulus. The main reward signal is fed into both amygdala and orbitofrontal cortex. A common output node exists for all model outputs, which is shown by E. Specifically, the node E accumulates the outputs of A nodes first; the inhibitory outputs of O nodes are then subtracted from this value [18].

The thalamic junctions are considered as the maximum of all stimulus and accounted as additional inputs for amygdala. The outputs of the internal areas are calculated by (12)–(14)

$$A_j = S_j V_j \tag{12}$$

$$O_j = S_j W_j \tag{13}$$

$$A_{\text{th}} = V_{\text{th}}.\{\max(S_j) = S_{\text{th}}\}. \tag{14}$$

The subscript j represents values regarding the jth input. The variations of V_j, W_j, and V_{th} in the learning process are calculated based on (15)–(17)

$$\Delta V_j = \gamma\left(\max\left(0, S_j\left(R - \sum_j A_j\right)\right)\right) \tag{15}$$

$$\Delta W_j = \delta \mathrm{S}_j\left(\sum_j A_j - \sum_j O_j - R\right) \tag{16}$$

$$\Delta V_{\text{th}} = \gamma_{\text{th}}(\max(0, S_{\text{th}}(R_e - A_{\text{th}}))). \tag{17}$$

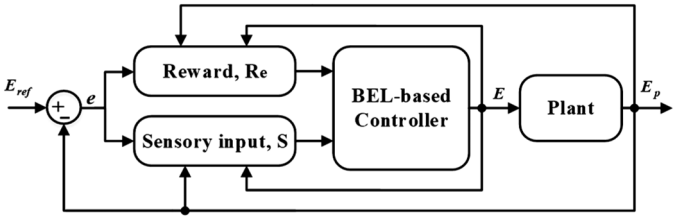

Fig. 7. Control system configuration.

The updated weights of V_j, W_j, and V_{th} can be calculated by

$$V_j(t) = \int_0^t \Delta V dt + V(0) \tag{18}$$

$$W_j(t) = \int_0^t \Delta W dt + W(0) \tag{19}$$

$$V_{\text{th}}(t) = \int_0^t \Delta V_{\text{th}} dt + V_{\text{th}}(0). \tag{20}$$

Finally, the model output is determined by (21)

$$E = \sum_j A_j + A_{\text{th}} - \sum_j O_j. \tag{21}$$

The values of A_j cannot be decreased, i.e., forgetting the learned information will not happen in amygdala, but in orbitofrontal cortex instead. Fig. 7 depicts the structure of the BEL-based controller. The emotional signal R_e and sensory inputs S are calculated by (22) and (23), respectively

$$R_e = f(E, e, E_p) \tag{22}$$

$$S = g(e, E_p, E). \tag{23}$$

In this article, f and g functions are selected based on the following equations:

$$g = k_1 e + k_2 \int e.dt \tag{24}$$

$$f = K_1 \mid e \mid + K_2 \mid e.E \mid + 0.5\max((\mid E_p \mid - E_{\max}), 0). \tag{25}$$

The controller gains for controlling flux, torque and speed are given in Table IV (Appendix II).

The values of γ, δ, initial values of A, A_{th}, O, and R_e and S functions must be appropriately designated. This control technique is an action-generation mechanism developed using emotional cues and sensory inputs.

To date, there is no established mathematical approach for tuning a BEL-based controller. In this study, we introduce an experimental tuning approach primarily through trial and error. The key principle is to select parameters that ensure the system's stability. When implementing the proposed method, the learning weights (V, W, and V_{th}) are continuously updated to track improvements. In response to sudden changes in the system,

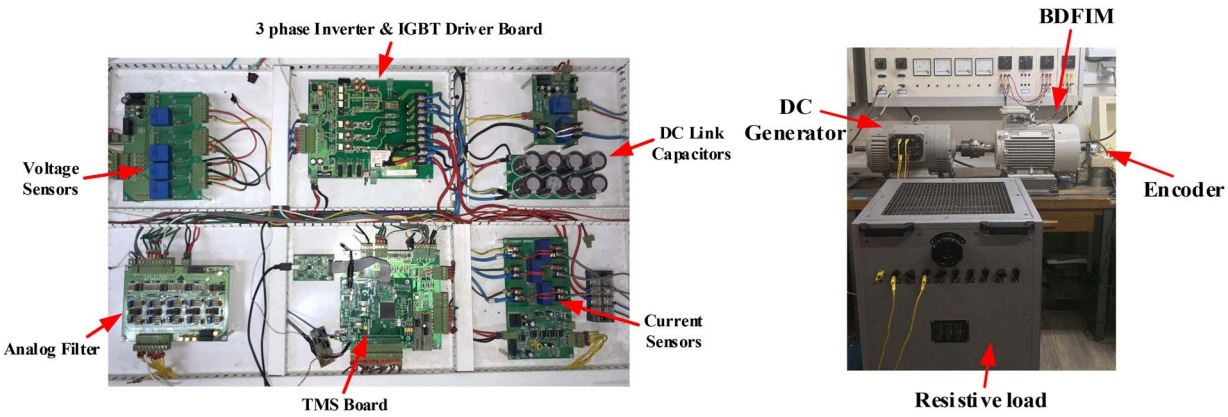

Fig. 8. BDFIM drive hardware.

these weights are adaptively tuned based on R_e and S signals. The tuning process for k_1, k_2, K_1, and K_2 is similar to that for coefficients of conventional PID controllers. k_1 and K_1 are related to adjusting the settling time, k_2 is responsible for smoothing the system response, and K_2 affects the steady-state error. To achieve the acceptable tracking performance, it is desirable that the controller and the system have matching dynamics. The proposed emotional controller has the flexibility to be programmed with any system dynamics by tuning the parameters, γ and γ_{th}: for slow dynamics, $\gamma > \gamma_{\text{th}}$; for fast dynamics, $\gamma < \gamma_{\text{th}}$, their absolute value should be each less than 1, and $0 < \delta < 1$.

IV. Results and Discussions

Fig. 8 shows the BDFIM drive hardware in the experimental setup: a BDFIM coupled to a dc generator; a 1024-pulse incremental encoder; the control drive system hardware, which includes six parts: an IGBT-based three-phase inverter with six gate drivers independently powering the machine, voltage and current sensors, an analog filter, dc-link capacitors, and a digital signal processor (DSP) TMS320F28335. The stator phase currents are measured by hall-effect current sensors (LEM LTS-6-NP). The three-phase voltages of stator windings are measured by voltage sensors (LEM LV-25-P). Table I shows specifications of the 3-kW prototype D132s-BDFIM used in experiments.

The block diagram in Fig. 9 shows integration of BEL-based controller into the MTPA controller for a BDFIM drive. For the outer loop, the input is the error signal between the reference speed with respect to the actual speed. For the inner loop, the inputs are two error signals: between the torque command and its actual value, and between the CW flux command and its actual value. Three EICs are involved in this control system: Two EICs receive the CW flux error and the torque error as the inputs and generate $u_1 = v_{2d}^*$ and $u_2 = v_{2q}^*$ as the outputs, respectively; and the 3rd EIC receives the speed error as the input and generates the torque command as the output (Fig. 10). The space vector modulation (SVM) technique is used to generate command voltages to control the inverter switches. Unlike conventional PI controllers, the proposed emotional control technique is auto-learning and model-free with adaptive controller coefficients, and enables independent control of BDFIMs regardless of the motor parameter variations.

TABLE I
Parameters of the D132 BDFIM Prototype Used in Experiments

Symbol	Value	Symbol	Value
V_1	180 (V) at 50 Hz	R_1	1.1237 (Ω)
V_2	180 (V) at 50 Hz	R_2	3.7171 (Ω)
T_e	20 (N.m)	R_r	1.3012 (Ω)
p_1	2	L_{1r}	0.1863 (H)
p_2	4	L_{2r}	0.0998 (H)
I_1	10 (A)	L_{l1}	0.0047 (H)
I_2	4.5 (A)	L_{l2}	0.0053 (H)
ω_n	500 (rpm)	L_{lr}	0.0206 (H)

According to the proposed flux search approach, when the CMA block detects a steady-state condition [Fig. 11(a)], the stepwise reduction of the CW reference flux starts. The CW flux is gradually adjusted to obtain the minimum current for $T_l = 0.6$ pu and $n_r = 1.3$ pu. Fig. 11(b) indicates that the CW reference flux has decreased from an initial value of 0.8 pu to a final value of 0.59 pu without instability. According to Fig. 11(c), as soon as it is detected that the decrease in flux has led to an increase in the total stator current, the MTPA controller adjusts the CW reference flux in the previous step to reach the optimum current point. Fig. 11(d) shows that the proposed controller provides a fast-tracking tuned response for the electromagnetic torque as the CW reference flux changes.

Fig. 12 shows the experimental stator current waveforms when the MTPA strategy is realized. Since the rotor speed is controlled at 0.72 pu, the frequency of the current waveforms at PW and CW are 50 Hz and 14 Hz, respectively, according to (8). Fig. 13 shows the state path of two-axis fluxes of CW under steady-state conditions experimentally. As expected, the curve drawn in the stationary reference frame is circle-shaped.

Fig. 14 shows the proposed drive system's response when the rotor speed reference varies from 1.06 pu to 1.1 pu exponentially, while the load torque remains constant. The reference speed equal to 1.06 pu corresponds to the CW reference flux set at its nominal value to provide fast dynamics of the system. After the MTPA controller detects that the rotor speed has reached a steady state, the flux reduction process begins until

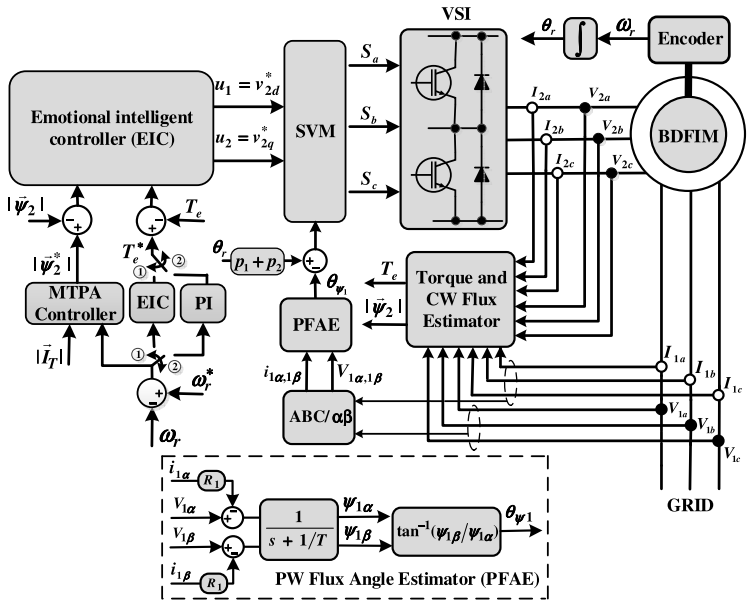

Fig. 9. Block diagram of the BDFIM-based drive system.

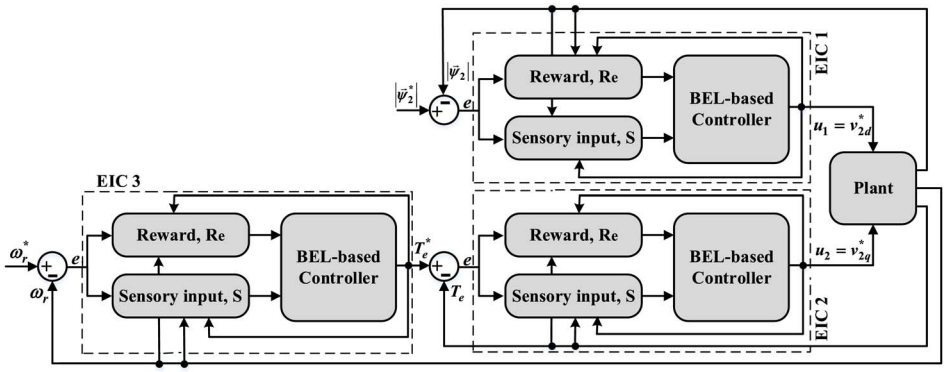

Fig. 10. Schematic representation of inputs and outputs of controllers.

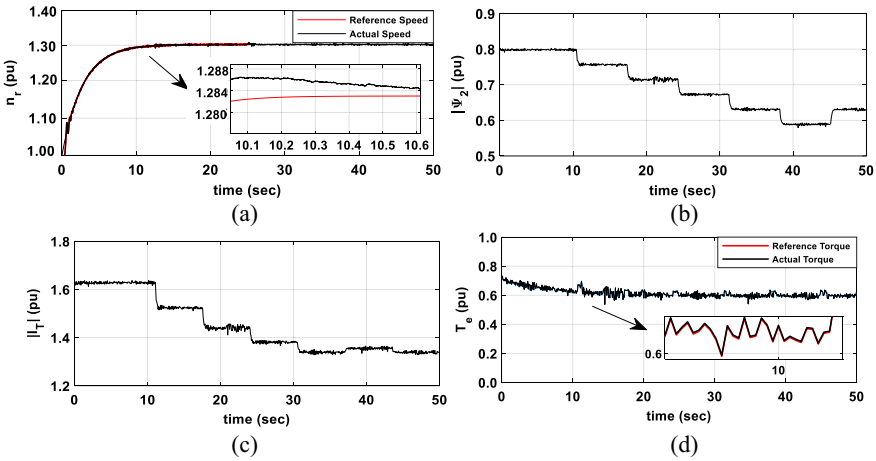

Fig. 11. Performance of the proposed control strategy through experiments. (a) Rotor speed. (b) CW flux adjusted by MTPA. (c) The total stator current with MTPA. (d) Electromagnetic torque.

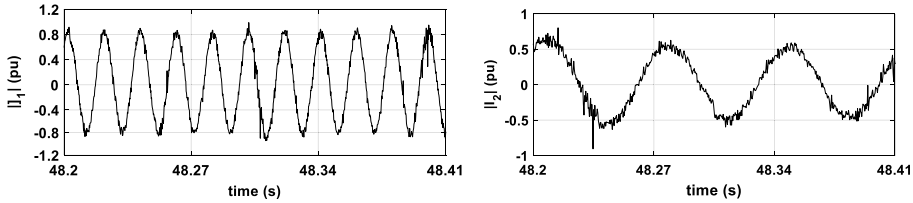

Fig. 12. Stator currents with MTPA. (a) PW current. (b) CW current.

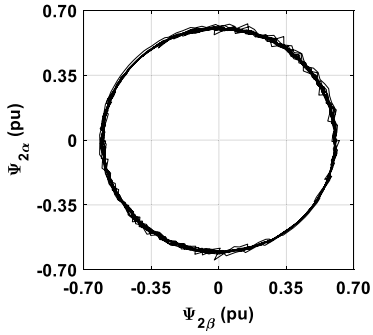

Fig. 13. CW flux trajectory obtained by experiments.

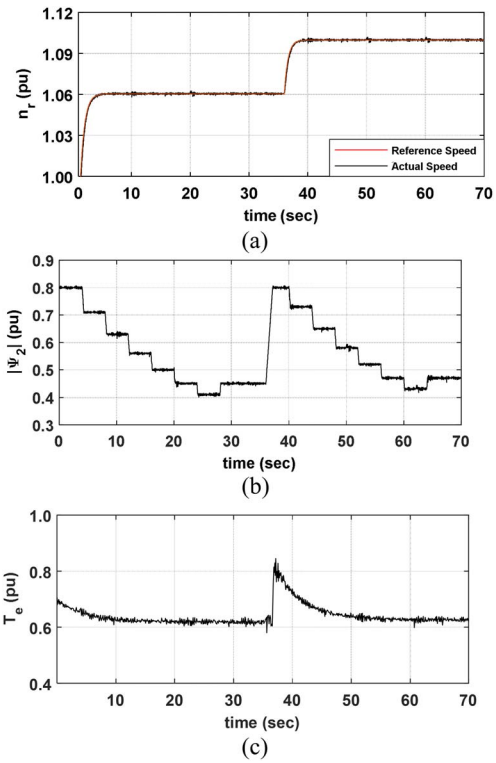

Fig. 14. Controller operation under a step change in the rotor speed reference through experiments. (a) Rotor speed. (b) CW flux. (c) Electromagnetic torque.

the total stator current reaches its minimum value. At $t = 37$ s, the rotor speed reference is changed, and the MTPA controller immediately raises the CW reference flux to its maximum value, so that the rotor speed follows its reference value with faster dynamics. As soon as a steady-state condition is detected around

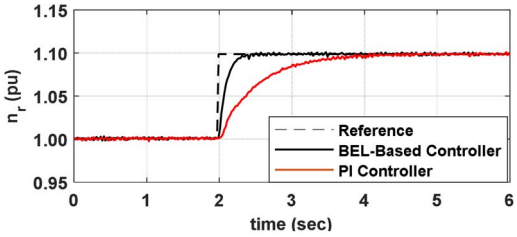

Fig. 15. Experimental speed control responses to a step change in the rotor speed reference for the proposed controller and a PI controller.

$t = 40$ s, the MTPA controller reduces the CW flux to minimize the total stator current at this new operating point. The speed control responses to a step change in the rotor speed reference for the proposed controller and a PI controller are shown in Fig. 15, where the load torque remains constant and the rotor speed is increased from the natural synchronous speed to track a step reference. To implement a PI controller for the speed control loop, the existing BEL-based speed controller in Fig. 10 is substituted by a PI controller.

To evaluate the performance of the speed controller, a test scenario is designed to let the rotor speed remain constant at 1.15 pu [Fig. 16(a)] and the load torque increased by 20% [Fig. 16(b)]. The proposed speed controller provides a fast tracking, small overshoots, and zero steady-state errors. In the proposed MTPA algorithm, the change in load torque is detected through the change of the total stator current over a certain time interval. Referring to Fig. 5, since the increase of load torque leads to a positive change in the total stator current, the CW flux is set at the rated value quickly to provide a fast dynamic [Fig. 16(c)]. Due to highly complex BDFIM models, all existing MTPA controllers for BDFIMs in the literature use model-based approaches with reduced-order machine models, such as the core model [34] and the fifth-order model [15], and using these simplified models decreases the MTPA control's accuracy. A less accurate model will cause the total stator current farther away from its actual minimum value. To reach its actual minimum value, one way is to use a model-free MTPA control. In Table II, the proposed model-free MTPA controller is compared with a model-based MTPA control using a fifth-order model of BDFIMs (taking iron losses into account) in [15] for different torques and rotor speeds. Table II shows the percent change of the total stator current for different torques and rotor speeds. Compared to the proposed controller, the controller in [15] results in an increase in the total stator current.

A comparison between the proposed BEL-based controller and a conventional PI controller [2] is shown in Table III. To

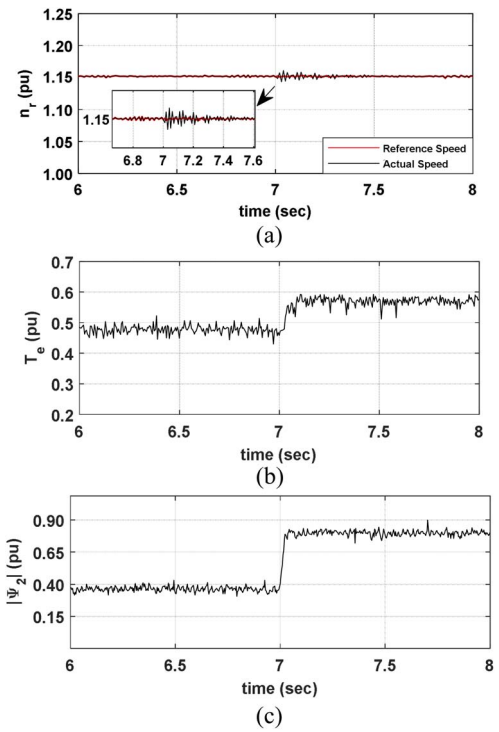

Fig. 16. Experimental performance of the proposed controller in the speed control loop with a 20% load torque increase. (a) Rotor speed. (b) Electromagnetic torque. (c) CW flux.

TABLE II
COMPARISON OF THE PROPOSED MODEL-FREE MTPA CONTROL AND THE MODEL-BASED MTPA CONTROL IN [15]: PERCENT CHANGE OF THE TOTAL STATOR CURRENT FOR DIFFERENT TORQUES AND ROTOR SPEEDS

	$T_l = 0.3$ pu	$T_l = 0.4$ pu	$T_l = 0.5$ pu
$n_r = 1.1$ pu	3.71%	3.50%	2.43%
$n_r = 1.2$ pu	3.38%	3.22%	2.37%
$n_r = 1.3$ pu	3.43%	3.83%	2.75%

$$\%\text{Percent change} = \frac{|I_T|_{[15]} - |I_T|_{\text{proposed}}}{|I_T|_{\text{proposed}}} \times 100$$

TABLE III
COMPARISON OF THE PROPOSED BEL-BASED SPEED CONTROLLER AND THE CONVENTIONAL PI CONTROLLER

The BEL-based speed controller	Conventional PI controller [2]
Zero steady state errors without under/over-shoot	Zero steady state errors, with under/ over-shoot
Fast dynamic response	Slow dynamic response
The d-q cross compensation is not required	The d-q cross compensation is required
Relatively complicated	Easy to use

evaluate the proposed controller, the simulation results of two scenarios with the load torque change [Fig. 17(a)] and the reference speed change [Fig. 17(b)] are illustrated, and the proposed controller shows superior performance. A simulation by MATLAB/Simulink is also conducted using specifications of a 22 kW BDFIM built at Cambridge University [32]. When the

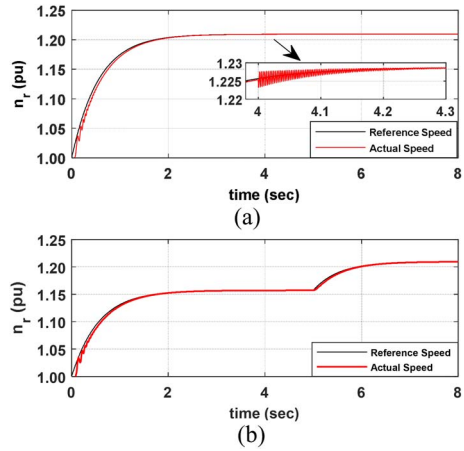

Fig. 17. Simulated response of the speed control system to changes in (a) load torque, (b) reference speed.

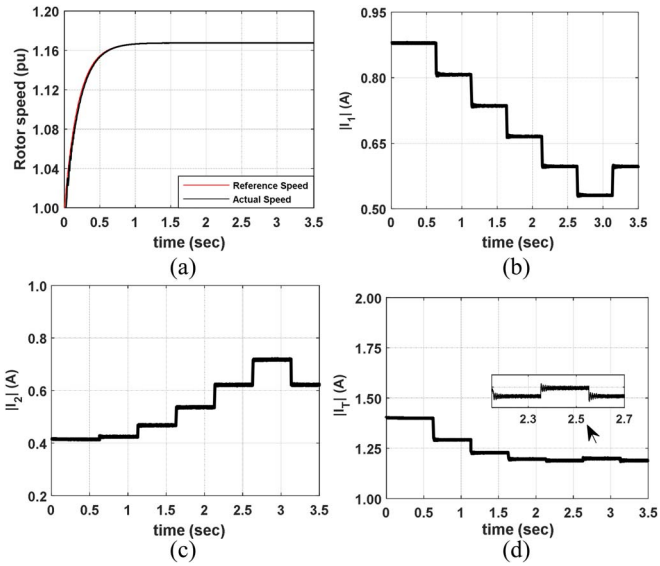

Fig. 18. Simulation results of the proposed MTPA control strategy. (a) Rotor speed. (b) PW current magnitude. (c) CW current magnitude. (d) The total stator current.

rotor speed error reaches a certain value (ε) [Fig. 18(a)], the MTPA control is initiated and the CW reference flux's magnitude is decreased step-by-step. This process continues until the total stator current is minimized. Through the MTPA control, although the PW current's magnitude reduction [Fig. 18(b)] is more significant than the CW current's magnitude increase [Fig. 18(c)], the sum of the stator current magnitudes is still minimized [Fig. 18(d)].

V. CONCLUSION

For brushless BDFIMs, all existing MTPA controllers in the literature are model-based using the reduced-order BDFIM model due to the machine's complexity. An alternative solution is to implement a search-based method, which can be adopted in various drive systems with different control schemes, thanks to its independency of machine

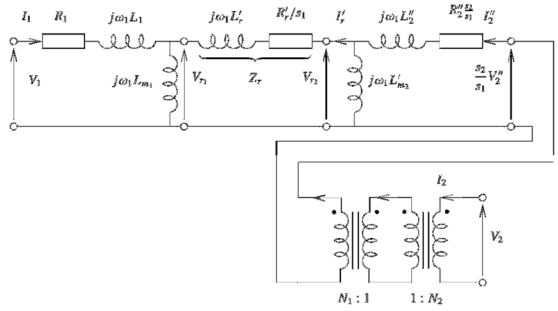

Fig. 19. BDFIM referred per phase equivalent circuit [32].

parameters and load conditions. In this article, a model-free MTPA controller for the BDFIM drive is developed for the first time, where the CW flux serves as the control variable. Through automatic step-by-step adjustments of this control variable, the total stator current can be minimized for the desired torque and rotor speed. The output of the MTPA controller is the CW reference flux. To generate the control inputs and apply them to the space vector modulation inverter, the error signals of the CW reference flux and the desired torque with respect to their actual values are delivered to the BEL-based controller. The proposed control scheme is completely model-free, simple to implement, and suitable for the BDFIM applications where the machine model is not available.

Appendix I

Based on Fig. 19, the relationship of the torque and stator currents of the BDFIM can be expressed as follows [34]:

$$T_e = -|\vec{I}_1|^2 L_{m1}^2 p_1 \frac{R_r'\omega_1}{|Z_r|^2} + |\vec{I}_2''|^2 L_{m2}'^2 p_2 \frac{R_r'\omega_1}{|Z_r|^2} + |\vec{I}_1||\vec{I}_2''| L_{m1}L_{m2}' \frac{\omega_1}{|Z_r|}((p_2-p_1)cos\Psi\cos(\theta_1+\theta_2) + (p_2+p_1)sin\Psi\sin(\theta_1+\theta_2)) \tag{A1}$$

where $|\vec{I}_i| = \sqrt{i_{id}^2 + i_{iq}^2}$, $\theta_i = \tan^{-1}\left(\frac{i_{iq}}{i_{id}}\right)$, $i = 1,2$ and $\Psi = \measuredangle Z_r$.

In the core model [35], the two stator currents, $|\vec{I}_1| \measuredangle\theta_1$ and $-|\vec{I}_2''| \measuredangle\theta_2$, are assumed equal (the uni-current proposition), and the torque equation can be simplified by [34]

$$|\vec{I}_1| = |\vec{I}_2''| = |\vec{I}| \Rightarrow |\vec{I}_2''| = \frac{N_1}{N_2}|\vec{I}| \tag{A2}$$

$$\theta_1 = \pi + \theta_2 \tag{A3}$$

$$T_e = |\vec{I}|^2 . \left(\frac{R_r'\omega_1}{|Z_r|^2}\left(\left(\frac{N_1}{N_2}\right)^2 L_{m2}^2 p_2 - L_{m1}^2 p_1\right) - \frac{N_1}{N_2}\frac{L_{m1}L_{m2}'\omega_1}{|Z_r|}((p_2-p_1)cos\Psi\cos(2\theta_1) + (p_2+p_1)sin\Psi\sin(2\theta_1))\right) \tag{A4}$$

To implement the MTPA concept in BDFIMs, Eq. (A.4) can be used by setting the optimal value of the current angle. In the search-based MTPA control, instead of the current angle, the flux is adjusted to obtain the minimum value of the total stator current for a given load torque. In this way, copper losses are minimized and the overall system efficiency is increased as long as copper losses are dominant [36].

Appendix II

TABLE IV
GAIN PARAMETERS FOR EICS

Flux control	$k_1 = 0.015$ $K_1 = 0.25$	$k_2 = 0.01$ $K_2 = 0.064$
Torque control	$k_1 = 0.01$ $K_1 = 0.18$	$k_2 = 0.01$ $K_2 = 0.045$
Speed control	$k_1 = 0.005$ $K_1 = 0.041$	$k_2 = 0.001$ $K_2 = 0.0021$

References

[1] H. Mosaddegh Hesar, H. A. Zarchi, and G. A. Markadeh, "Modeling and dynamic performance analysis of brushless doubly fed induction machine considering iron loss," *IEEE Trans. Energy Convers.*, vol. 35, no. 1, pp. 193–202, Mar. 2020.

[2] J. Poza, E. Oyarbide, I. Sarasola, and M. Rodriguez, "Vector control design and experimental evaluation for the brushless doubly fed machine," *IET Electric Power Appl.*, vol. 3, no. 4, pp. 247–256, Jul. 2009.

[3] H. Mosaddegh Hesar, X. Liang, H. A. Zarchi, H. Chenarani, and A. Khazaee, "High-efficient nonlinear control for brushless doubly-fed induction machines," *IEEE Trans. Energy Convers.*, vol. 38, no. 2, pp. 1442–1451, Jun. 2023.

[4] H. Mosaddegh Hesar, H. A. Zarchi, and G. A. Markadeh, "Stator flux oriented control of brushless doubly fed induction motor drives based on maximum torque per total ampere strategy," in *Proc. 10th Int. Power Electron., Drive Syst. Technol. Conf. (PEDSTC)*, Shiraz, Iran, 2019, pp. 84–89.

[5] I. Sarasola, J. Poza, M. A. Rodriguez, and G. Abad, "Direct torque control design and experimental evaluation for the brushless doubly fed machine," *Energy Convers. Manage.*, vol. 52, no. 2, pp. 1226–1234, Feb. 2011.

[6] E. Daryabeigi, H. Abootorabi Zarchi, G. R. Arab Markadeh, J. Soltani, and F. Blaabjerg, "Online MTPA control approach for synchronous reluctance motor drives based on emotional controller," *IEEE Trans. Power Electron.*, vol. 30, no. 4, pp. 2157–2166, Apr. 2015.

[7] H. Mosaddegh Hesar, H. Abootorabi Zarchi, and M. Ayaz Khoshhava, "Online maximum torque per ampere control for induction motor drives considering iron loss using input–output feedback linearisation," *IET Electric Power Appl.*, vol. 13, no. 12, pp. 2113–2120, Nov. 2019.

[8] A. Shawier, A. S. Abdel-Khalik, R. A. Hamdy, K. H. Ahmed, and S. Ahmed, "Post fault operation of five-phase induction machine with minimum total losses under single open-phase fault," *IEEE Access*, vol. 8, pp. 208696–208706, 2020.

[9] G. Feng, C. Lai, Y. Han, and N. C. Kar, "Fast maximum torque per ampere (MTPA) angle detection for interior PMSMs using online polynomial curve fitting," *IEEE Trans. Power Electron.*, vol. 37, no. 2, pp. 2045–2056, Feb. 2022.

[10] R. E. Betz and M. G. Jovanovic, "Theoretical analysis of control properties for the brushless doubly fed reluctance machine," *IEEE Trans. Energy Convers.*, vol. 17, no. 3, pp. 332–339, Sep. 2002.

[11] S. Ademi and M. Jovanović, "Maximum torque per inverter ampere control of brushless doubly-fed reluctance generators for wind turbines," in *Proc. Int. Symp. Power Electron., Elect. Drives, Automat. Motion*, Aug. 2014, pp. 883–888.

[12] S. Ademi and M. G. Jovanović, "Vector control methods for brushless doubly fed reluctance machines," *IEEE Trans. Ind. Electron.*, vol. 62, no. 1, pp. 96–104, Jan. 2015.

[13] S. Ademi, M. G. Jovanović, H. Chaal, and W. Cao, "A new sensorless speed control scheme for doubly fed reluctance generators," *IEEE Trans. Energy Convers.*, vol. 31, no. 3, pp. 993–1001, Sep. 2016.
[14] H. Mosaddegh Hesar, H. Abootorabi Zarchi, and G. Arab Markadeh, "Online MTPTA and MTPIA control of brushless doubly fed induction motor drives," *IEEE Trans. Power Electron.*, vol. 36, no. 1, pp. 691–701, Jan. 2021.
[15] H. Mosaddegh Hesar, H. Abootorabi Zarchi, G. Arab Markadeh, and A. Khazaee, "Maximum torque per total ampere strategy for vector-controlled brushless doubly fed induction machine drive taking iron loss into account," *IEEE Trans. Power Electron.*, vol. 37, no. 11, pp. 13598–13605, Nov. 2022.
[16] G. Zhang et al., "A robust control scheme based on ISMC for the brushless doubly fed induction machine," *IEEE Trans. Power Electron.*, vol. 33, no. 4, pp. 3129–3140, Apr. 2018.
[17] X. Yan and M. Cheng, "A robustness-improved control method based on ST-SMC for cascaded brushless doubly fed induction generator," *IEEE Trans. Ind. Electron.*, vol. 68, no. 8, pp. 7061–7071, Aug. 2021.
[18] G. R. Markadeh, E. Daryabeigi, C. Lucas, and M. A. Rahman, "Speed and flux control of induction motors using emotional intelligent controller," *IEEE Trans. Ind. Appl.*, vol. 47, no. 3, pp. 1126–1135, May/Jun. 2011.
[19] H. A. Zarchi, E. Daryabeigi, G. R. A. Markadeh, and J. Soltani, "Emotional controller (BELBIC) based DTC for encoderless synchronous reluctance motor drives," in *Proc. 2nd Power Electron., Drive Syst. Technol. Conf.*, Feb. 2011, pp. 478–483.
[20] C. Lucas, D. Shahmirzadi, and N. Sheikholeslami, "Introducing BELBIC: Brain emotional learning-based intelligent control," *Intell. Automat. Soft Comput.*, vol. 10, no. 1, pp. 11–22, Jan. 2004.
[21] M. R. Jamali, M. Dehyadegari, A. Arami, C. Lucas, and Z. Navabi, "Real time embedded emotional controller," *Neural Comput. Appl.*, vol. 19, no. 1, pp. 13–19, Feb. 2010.
[22] M. A. Rahman, R. M. Milasi, C. Lucas, B. N. Arrabi, and T. S. Radwan, "Implementation of emotional controller for interior permanent magnet synchronous motor drive," *IEEE Trans. Ind. Appl.*, vol. 44, no. 5, pp. 1466–1476, Sep./Oct. 2008.
[23] M. Abshari, H. H. Safa, and S. M. Saghaiannejad, "Indirect torque control of SRM by intelligent controller with considering torque ripple reduction," in *Proc. 8th Power Electron., Drive Syst. Technol. Conf. (PEDSTC)*, Feb. 2017, pp. 270–275.
[24] A. M. Yazdani et al., "Intelligent speed control of hybrid stepper motor considering model uncertainty using brain emotional learning," *Can. J. Elect. Comput. Eng.*, vol. 41, no. 2, pp. 95–104, Aug. 2018.
[25] E. Daryabeigi, A. Mirzaei, H. Abootorabi Zarchi, and S. Vaez-Zadeh, "Enhanced emotional and speed deviation control of synchronous reluctance motor drives," *IEEE Trans. Energy Convers.*, vol. 34, no. 2, pp. 604–612, Jun. 2019.
[26] M. Qutubuddin, T. K. Gibo, R. S. Bapi, and Y. Narri, "Brain affective system inspired control architecture: An application to nonlinear system," *IEEE Access*, vol. 9, pp. 86565–86580, 2021.
[27] M. A. Khoshhava, H. Abootorabi Zarchi, and H. M. Hesar, "Direct torque and flux control of dual stator winding induction motor drives based on emotional controller," in *Proc. 27th Iranian Conf. Elect. Eng. (ICEE)*, Yazd, Iran, 2019, pp. 720–724.
[28] S. Williamson, A. C. Ferreira, and A. Wallace, "Generalized theory of the brushless doubly-fed machine-part I: Analysis," *IEEE Electric Power Appl.*, vol. 144, no. 2, pp. 111–122, Mar. 1997.
[29] S. Abdi, E. Abdi, and R. McMahon, "A study of unbalanced magnetic pull in brushless doubly-fed machines," *IEEE Trans. Energy Convers.*, vol. 30, no. 3, pp. 1218–1227, Sep. 2015.
[30] S. Tohidi, H. Oraee, M. R. Zolghadri, S. Shao, and P. Tavner, "Analysis and enhancement of low-voltage ride-through capability of brushless doubly fed induction generator," *IEEE Trans. Ind. Electron.*, vol. 60, no. 3, pp. 1146–1155, Mar. 2013.
[31] H. Mosaddegh Hesar, X. Liang, M. A. Salahmanesh, M. A. Khoshhava, and S. Abdi, "Vector control of brushless doubly-fed induction machines based on highly efficient nonlinear controllers," *IEEE Trans. Ind. Electron.*, vol. 71, no. 6, pp. 5641–5652, Jun. 2024.
[32] P. Roberts, "A study of brushless doubly-fed (induction) machines," Ph.D. diss., Univ. Cambridge, Cambridge, U.K., Sep. 2004.
[33] M. A. Khoshhava, H. A. Zarchi, G. R. A. Markadeh, H. Mosaddegh Hesar, and K. Al-Haddad, "A novel highly efficient torque sharing algorithm for dual stator winding induction machines for various speed regions," *IEEE Trans. Ind. Electron.*, vol. 71, no. 6, pp. 5564–5575, Jun. 2024.
[34] M. Ahmadian, B. Jandaghi, and H. Oraee, "Maximum torque per ampere operation of brushless doubly fed induction machines," *Renewable Energies Power Qual. J.*, vol. 1, no. 9, pp. 981–985, May 2011.
[35] R. A. McMahon, P. C. Roberts, X. Wang, and P. J. Tavner, "Performance of BDFM as generator and motor," *IEE Electric Power Appl.*, vol. 153, no. 2, pp. 289–299, Mar. 2006.
[36] S. Bolognani, L. Peretti, and M. Zigliotto, "Online MTPA control strategy for DTC synchronous-reluctance-motor drives," *IEEE Trans. Power Electron.*, vol. 26, no. 1, pp. 20–28, Jan. 2011.

Hamidreza Mosaddegh-Hesar (Member, IEEE) received the Ph.D. degree in electrical engineering from Ferdowsi University of Mashhad, Mashhad, Iran, in 2019.

He is currently working as a Postdoctoral Fellow with the Power and Energy Conversion Laboratory, University of Saskatchewan, Saskatoon, Canada. He serves as an Associate Editor for IEEE TRANSACTIONS ON INDUSTRY APPLICATIONS.

Xiaodong Liang (Senior Member, IEEE) was born in Lingyuan, Liaoning, China. She received the B.Eng. and M.Eng. degrees from Shenyang Polytechnic University, Shenyang, China, in 1992 and 1995, respectively, the M.Sc. degree from the University of Saskatchewan, Saskatoon, Canada, in 2004, and the Ph.D. degree from the University of Alberta, Edmonton, Canada, in 2013, all in electrical engineering.

From 1995 to 1999, she served as a Lecturer with Northeastern University, Shenyang, China. In 2001, she joined Schlumberger (SLB) in Edmonton, Canada, and was promoted to a Principal Power Systems Engineer with the world's leading oil field service company in 2009. She worked with Schlumberger for almost 12 years until 2013. From 2013 to 2019, she was with Washington State University in Vancouver, WA, USA, and Memorial University of Newfoundland in St. John's, NL, Canada, as an Assistant Professor and later an Associate Professor. In 2019, she joined the University of Saskatchewan, where she is currently a Professor and Canada Research Chair in Technology Solutions for Energy Security in Remote, Northern, and Indigenous Communities. She was an Adjunct Professor with Memorial University of Newfoundland from 2019 to 2022. Her research interests include power systems, renewable energy, and electric machines.

Dr. Liang is a registered Professional Engineer in the province of Saskatchewan, Canada, a Fellow of IET, and Deputy Editor-in-Chief of IEEE TRANSACTIONS ON INDUSTRY APPLICATIONS.

Hossein Abootorabi Zarchi received the M.S. and Ph.D. degrees in electrical engineering from Isfahan University of Technology, Isfahan, Iran, in 2004 and 2010, respectively.

He was a Visiting Ph.D. Student with the Control and Automation Group, Denmark Technical University, Denmark, from 2009 to 2010. He is currently an Associate Professor with the Department of Electrical Engineering, Ferdowsi University of Mashhad, Mashhad, Iran. His research interests include electrical machines, nonlinear control of motor drives and renewable energies.

Mojtaba Ayaz Khoshhava (Member, IEEE) received the M.S. degree from Shiraz University, Shiraz, Iran, in 2024, and the Ph.D. degree from Ferdowsi University of Mashhad, Mashhad, Iran, in 2020, all in electrical engineering.

He is currently a Postdoctoral Fellow with École de Technologie Supérieure (ÉTS), Montreal, Canada. His main research interests include electrical machines control, design, and modeling.

Amir Khazaee received the Ph.D. degree in electrical engineering from Ferdowsi University of Mashhad, Mashhad, Iran, in 2019.

From 2017 to 2022, he was with Mashhad Electric Energy Distribution Co., Mashhad, Iran. From 2022 to 2023, he was working as a Postdoctoral Fellow with the Laboratory for Electric Drive Application and Research (LEDAR), Toronto Metropolitan University, Toronto, ON, Canada. Since 2023, he is working with École de Technologie Supérieure (ÉTS), Montreal, Canada. His research interests include electrical machines control and modelling.